View metadata, citation and similar papers at core.ac.uk

brought to you by CORE

provided by UNL | Libraries

University of Nebraska - Lincoln

DigitalCommons@University of Nebraska - Lincoln

Faculty Publications, Department of Physics and Astronomy

Research Papers in Physics and Astronomy

2013

EPR identification of defects responsible for thermoluminescence in Cu-doped lithium tetraborate ($Li_2B_4O_7$) crystals

A. T. Brant

D. A. Buchanan

J. W. McClory

P. A. Dowben

V. T. Adamiv

See next page for additional authors

Follow this and additional works at: https://digitalcommons.unl.edu/physicsfacpub

This Article is brought to you for free and open access by the Research Papers in Physics and Astronomy at DigitalCommons@University of Nebraska - Lincoln. It has been accepted for inclusion in Faculty Publications, Department of Physics and Astronomy by an authorized administrator of DigitalCommons@University of Nebraska - Lincoln.

Authors

A. T. Brant, D. A. Buchanan, J. W. McClory, P. A. Dowben, V. T. Adamiv, Ya. V. Burak, and L. E. Halliburton

Journal of Luminescence 139 (2013) 125–131

Contents lists available at SciVerse ScienceDirect

Journal of Luminescence

journal homepage: www.elsevier.com/locate/jlumin

EPR identification of defects responsible for thermoluminescence in Cu-doped lithium tetraborate ($Li_2B_4O_7$) crystals

A.T. Brant [a,*], D.A. Buchanan [a], J.W. McClory [a], P.A. Dowben [b], V.T. Adamiv [c], Ya.V. Burak [c], L.E. Halliburton [d]

[a] Department of Engineering Physics, Air Force Institute of Technology, Wright-Patterson Air Force Base, OH 45433, USA
[b] Department of Physics and Astronomy, Nebraska Center for Materials and Nanoscience, University of Nebraska, Lincoln, Nebraska 68588, USA
[c] Institute of Physical Optics, 23 Dragomanov St., Lviv 79005, Ukraine
[d] Department of Physics, West Virginia University, Morgantown, WV 26505, USA

ARTICLE INFO

Article history:
Received 18 October 2012
Received in revised form
25 January 2013
Accepted 12 February 2013
Available online 21 February 2013

Keywords:
Lithium tetraborate
Electron paramagnetic resonance
Copper doping
Crystal defects
Radiation dosimetry
Thermoluminescence

ABSTRACT

Electron paramagnetic resonance (EPR) is used to identify the electron and hole traps responsible for thermoluminescence (TL) peaks occurring near 100 and 200 °C in copper-doped lithium tetraborate ($Li_2B_4O_7$) crystals. As-grown crystals have Cu^+ and Cu^{2+} ions substituting for lithium and have Cu^+ ions at interstitial sites. All of the substitutional Cu^{2+} ions in the as-grown crystals have an adjacent lithium vacancy and give rise to a distinct EPR spectrum. Exposure to ionizing radiation at room temperature produces a second and different Cu^{2+} EPR spectrum when a hole is trapped by substitutional Cu^+ ions that have no nearby defects. These two Cu^{2+} trapped-hole centers are referred to as Cu^{2+}-V_{Li} and Cu^{2+}_{active}, respectively. Also during the irradiation, two trapped-electron centers in the form of interstitial Cu^0 atoms are produced when interstitial Cu^+ ions trap electrons. They are observed with EPR and are labeled Cu^0_A and Cu^0_B. When an irradiated crystal is warmed from 25 to 150 °C, the Cu^{2+}_{active} centers have a partial decay step that correlates with the TL peak near 100 °C. The concentrations of Cu^0_A and Cu^0_B centers, however, increase as the crystal is heated through this range. As the crystal is further warmed between 150 and 250 °C, the EPR signals from the Cu^{2+}_{active} hole centers and Cu^0_A and Cu^0_B electron centers decay simultaneously. This decay step correlates with the intense TL peak near 200 °C.

Published by Elsevier B.V.

1. Introduction

Lithium tetraborate ($Li_2B_4O_7$) crystals doped with copper, silver, or other transition-metal ions are important candidates for thermoluminescence (TL) dosimetry applications. Radiative processes associated with these dopants are efficient, and bright above-room-temperature TL peaks are observed. These crystals also have potential for use as neutron detectors because ^6Li and ^{10}B have large capture-cross-sections for thermal neutrons. During the last several decades, there have been numerous studies of photoluminescence [1–5] and thermoluminescence [6–18] from $Li_2B_4O_7$ crystals. Other reports [19–25] describe radiation-induced defects and explore the effects of radiation on the optical properties of $Li_2B_4O_7$. Many investigations have focused on copper, silver, and manganese impurity ions. These dopants are easily incorporated into a crystal during growth, and they greatly increase the TL light output. Takenaga and coworkers [26] were the first to investigate the TL properties of copper-doped $Li_2B_4O_7$ crystals. They found that crystals doped with copper exhibited higher TL sensitivity than crystals doped with manganese. Copper-doped crystals also have linear TL output with radiation exposure up to 10^5 R and low loss of sensitivity due to humidity. The emitted light from Cu-doped crystals is near the blue end of the visible spectrum [17]. This matches the optimum sensitivity of photomultiplier tubes and makes these crystals well-suited for dosimetry and radiation-detection applications.

A recent electron paramagnetic resonance (EPR) and electron-nuclear double resonance (ENDOR) study by Swinney et al. [27] showed that as-grown undoped $Li_2B_4O_7$ crystals contain large concentrations of oxygen vacancies and lithium vacancies. In the as-grown crystals, these vacancies prefer to be in nonparamagnetic forms (with no trapped electrons or holes). They have opposite "effective" charges and thus act as charge compensators for each other (two lithium vacancies compensate one oxygen vacancy). During an irradiation at low temperature (i.e., near 77 K), these vacancies are the dominant radiation-induced electron and hole traps, respectively, in undoped crystals. The trapped-electron center (an oxygen vacancy with one trapped

* Corresponding author. Tel.: +1 937 255 3636x4741
E-mail address: Adam.Brant.ctr@afit.edu (A.T. Brant).

0022-2313/$ - see front matter Published by Elsevier B.V.
http://dx.doi.org/10.1016/j.jlumin.2013.02.023

This document is a U.S. government work and is not subject to copyright in the United States.

electron) is thermally stable at room temperature, but the trapped-hole center (a lithium vacancy with a hole trapped on an adjacent oxygen ion) rapidly decays when the temperature is raised above 100 K. This lack of a trapped hole center and the related lack of a radiatively efficient recombination center explains why there are no strong TL peaks above room temperature in undoped $Li_2B_4O_7$ crystals. The situation changes, however, when the crystal is doped with copper. In these crystals, Cu^+ ions substitute for Li^+ ions and also occupy interstitial sites. The Cu^+ ions at the interstitial sites provide charge compensation for lithium vacancies. Together, these effects suggest that doping with copper will reduce the concentrations of the isolated oxygen vacancies and lithium vacancies that form during growth. By extension, this means that the copper ions must assume the roles of both electron trap and hole trap in order to have an intense above-room-temperature TL peak in Cu-doped $Li_2B_4O_7$ crystals. It is widely accepted that the substitutional Cu^{2+} ions are the primary trapped-hole center, but thus far, no direct experimental evidence for the identity of the primary trapped-electron centers has been available. Substitutional Cu^+ ions could act as the electron trap (i.e., the substitutional Cu^+ ions could be amphoteric), but substitutional Cu^0 centers would be relatively shallow and are not expected to be stable above room temperature. We point out that a similar problem has been addressed in the EPR and ENDOR study of Ag-doped $Li_2B_4O_7$ crystals by Brant et al. [28]. Substitutional Ag^{2+} hole traps and interstitial Ag^0 electron traps, both radiation-induced, were identified by those investigators, and a pulsed anneal verified that the thermal decay of the EPR signals from the Ag^{2+} and Ag^0 centers coincided with an intense above-room-temperature TL peak.

In the present investigation of $Li_2B_4O_7$, EPR is used to identify and characterize a new radiation-induced Cu^{2+} trapped-hole center (labeled Cu^{2+}_{active}) and two new radiation-induced interstitial Cu^0 trapped-electron centers (labeled Cu^0_A and Cu^0_B). These three trapping centers have not been previously reported in the literature. Prior to an irradiation with X-rays, an EPR spectrum assigned to Cu^{2+} ions with an adjacent lithium vacancy is observed. This spectrum, present in as-grown crystals, has been reported by Corradi et al. [29,30]. When a Cu-doped $Li_2B_4O_7$ crystal is exposed to x rays at room temperature, a portion of the isolated substitutional Cu^+ ions trap a hole and form Cu^{2+} hole centers (Cu^{2+}_{active}). At the same time, a portion of the interstitial Cu^+ ions trap electrons and form two distinct Cu^0 electron centers (Cu^0_A and Cu^0_B). The thermal stabilities of these radiation-induced Cu-related defects are determined by performing isochronal anneals at progressively higher temperatures and observing their effect on the intensity of the EPR signals. Decay steps of the Cu^{2+}_{active} center correlate with the two above-room-temperature TL peaks, one near 100 °C and the other near 200 °C. The concentration of Cu^0_A and Cu^0_B centers, however, increases as the crystal is warmed from room temperature to 125 °C. This suggests that electrons are thermally released from a third unidentified defect (possibly oxygen vacancies). Some of these released electrons recombine with the radiation-induced trapped holes and give rise to the TL peak near 100 °C, while the rest of the released electrons are trapped and form the Cu^0_A and Cu^0_B centers. As the crystal is warmed from 150 to 250 °C, the Cu^0_A and Cu^0_B electron centers and Cu^{2+}_{active} hole centers decay at the same time, and this electron–hole recombination produces the TL peak near 200 °C.

2. Experimental

The Cu-doped $Li_2B_4O_7$ single crystal used in this study was grown by the Czochralski technique at the Institute of Physical Optics (L'viv, Ukraine). The copper dopant level in the starting material was 0.015 at%. EPR samples with dimensions of approximately $2 \times 3 \times 1$ mm^3 were cut from the larger boule. $Li_2B_4O_7$ crystals have tetragonal symmetry (space group $I4_1cd$) with lattice constants $a = 9.475$ Å and $c = 10.283$ Å [31–34]. In this lattice, each lithium ion has five nearest-neighbor oxygen ions, and all lithium sites are crystallographically equivalent. The basic building-block is the $(B_4O_9)^{6-}$ covalent unit that is composed of two BO_3 and two BO_4 units. A schematic representation of the crystal structure is presented in Fig. 1, showing the $(B_4O_9)^{6-}$ unit and one adjacent lithium ion with its five nearest neighbor oxygen ions [33,34].

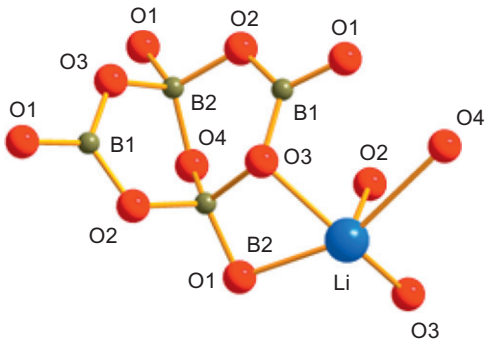

Fig. 1. An arbitrary projection of a portion of the $Li_2B_4O_7$ crystal lattice. The basic B_4O_9 unit and the five oxygen ions neighboring a lithium site are shown. The ion labeling scheme follows the convention of Refs. [27,28,33,34].

EPR data were taken using a Bruker EMX spectrometer operating near 9.4 GHz. Low temperatures (25–45 K) were achieved with an Oxford helium-gas flow system. A proton NMR gaussmeter was used to measure the static magnetic field and a MgO:Cr^{3+} crystal ($g = 1.9800$) provided corrections for the small difference in field strength between the gaussmeter probe tip and the sample. Samples were X-ray-irradiated at room temperature with a tube operating at 50 kV. Irradiation times were 60 min. The X-rays did not produce any noticeable change in the color of the crystals.

Thermoluminescence glow curves were taken using a Harshaw TLD-3500 reader. This reader detected the total light output using a photomultiplier tube. The spectral dependence of the emitted light was not obtained. In order to minimize the effect of optical and thermal fading, TL data were taken within a few hours of an X-ray irradiation, and the sample was kept in the dark prior to the TL measurements.

3. EPR and TL results

3.1. Radiation-induced Cu^{2+} centers

Prior to an irradiation with X-rays, our copper-doped $Li_2B_4O_7$ sample contained a large concentration of Cu^{2+} ($3d^9$) ions, as shown by the intense EPR spectrum in Fig. 2(a). These data were taken at 25 K with the magnetic field parallel to the [1 1 0] direction in the crystal. Corradi et al. [29] first reported this Cu^{2+} signal and performed a complete angular dependence study to determine the principal values and principal-axis directions of the g matrix and the Cu-hyperfine matrices. We assign the EPR spectrum in Fig. 2(a) to a substitutional Cu^{2+} ion on a Li^+ cation site, with charge compensation provided by an adjacent lithium vacancy. We refer to this defect as the Cu^{2+}-V_{Li} center. The Cu^{2+}-V_{Li} center has eight crystallographically equivalent orientations in the tetragonal $Li_2B_4O_7$ lattice. When the magnetic field is aligned along the [1 1 0] direction, these eight sites separate into two magnetically inequivalent sets, each with fourfold degeneracy. The two sets of lines associated with the Cu^{2+}-V_{Li} defect are indicated by the upper stick diagram in Fig. 2(a). Copper has two magnetic isotopes, ^{63}Cu (69.2% abundant) and ^{65}Cu (30.8%

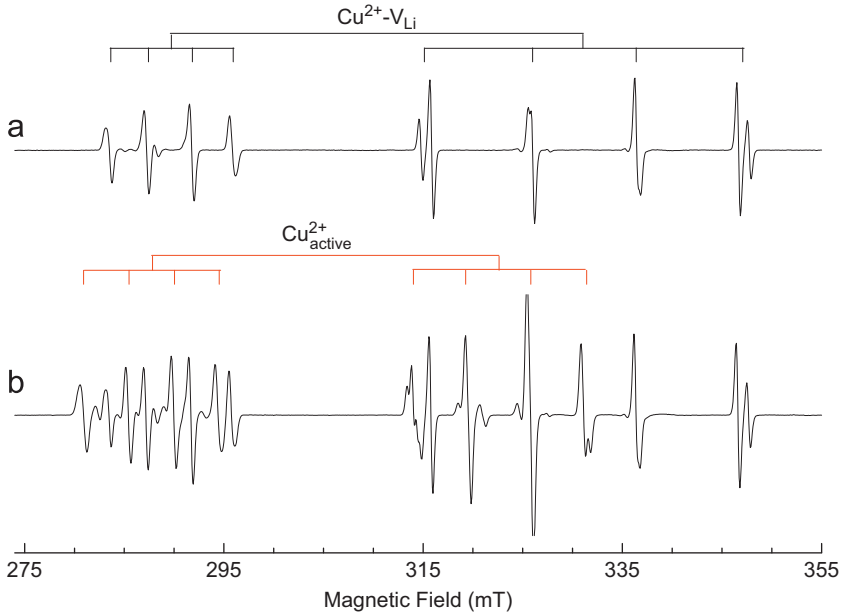

Fig. 2. EPR spectra illustrating the production of the Cu^{2+}_{active} center. These data were taken at 25 K with the magnetic field aligned along the [1 1 0] direction. (a) This spectrum was taken prior to irradiation and shows only the Cu^{2+}-V_{Li} center. (b) This spectrum was taken after an X-ray irradiation at room temperature and shows both the Cu^{2+}-V_{Li} center and the Cu^{2+}_{active} center. The stick diagrams indicate the averaged positions of the ^{63}Cu and ^{65}Cu lines. (For interpretation of the references to color in this figure, the reader is referred to the web version of this article.)

abundant), both with $I=3/2$. The magnetic moments of ^{63}Cu and ^{65}Cu are similar (with ^{65}Cu being slightly larger), so the lines associated with the separate isotopes are not always resolved (this is the case in the lower-field set in Fig. 2(a)). In the high-field set, the outer ^{63}Cu and ^{65}Cu lines are resolved and the inner lines near 326 and 337 mT are distorted due to the overlap of ^{63}Cu and ^{65}Cu lines. The upper stick diagram in Fig. 2(a) indicates the averaged positions of the ^{63}Cu and ^{65}Cu hyperfine lines.

The spectrum in Fig. 2(b) was taken after our Cu-doped $Li_2B_4O_7$ crystal was exposed to x rays at room temperature. This spectrum was also taken at 25 K with the magnetic field along the [1 1 0] direction, and thus can be directly compared to the spectrum in Fig. 2(a). The EPR signal intensity of the Cu^{2+}-V_{Li} center does not change with irradiation. We do, however, see a new Cu^{2+} center appear in the same magnetic field region as the Cu^{2+}-V_{Li} center. The red stick diagram in Fig. 2(b) identifies the two magnetically inequivalent orientations of this new Cu^{2+} center. The g matrix and the hyperfine matrices for the Cu^{2+}-V_{Li} center and this new Cu^{2+} center are similar. We assign the new defect to a substitutional Cu^{2+} ion replacing a Li^+ ion with no other defects nearby, and refer to it as the active Cu^{2+} center (Cu^{2+}_{active}). The lines from the two magnetic copper isotopes are not resolved in the Cu^{2+}_{active} spectrum shown in Fig. 2(b), although the highest-field ^{65}Cu line is partially visible near 332 mT. The Cu^{2+}_{active} defect is produced when an isolated substitutional Cu^+ ion traps a hole during the irradiation, thus forming a Cu^{2+} ion. In Fig.2(b), the concentration of Cu^{2+}-V_{Li} centers and radiation-induced Cu^{2+}_{active} centers are nearly the same (their individual concentrations are estimated to be 2.1×10^{18} cm^{-3}). Thus, as observed with EPR, the production of the radiation-induced Cu^{2+}_{active} center nearly doubles the overall concentration of Cu^{2+} ions in the crystal. Unlike the Cu^{2+}-V_{Li} center, the radiation-induced Cu^{2+}_{active} center does not have a neighboring lithium vacancy for charge compensation. Instead, it is charge compensated nonlocally by an interstitial Cu^0 atom that forms when an interstitial Cu^+ ion traps an electron during the irradiation (see Section 3.2). This difference in the surrounding environment of the Cu^{2+}-V_{Li} and the Cu^{2+}_{active} centers slightly changes the g values and ^{63,65}Cu hyperfine parameters and causes the similar, yet distinct, EPR spectra seen in Fig. 2(b).

3.2. Radiation-induced Cu^0 centers

Copper ions also play the role of electron trap in doped $Li_2B_4O_7$ crystals. Fig. 3 shows two previously unreported EPR spectra, representing defects that we label Cu^0_A and Cu^0_B. These data were taken at 45 K with the magnetic field along the [0 0 1] direction. The Cu^0_A and Cu^0_B signals were not present prior to the irradiation with x rays. The spectra from the Cu^0_A and Cu^0_B centers are complex. The four widely separated groups of lines in Fig. 3, indicated by red and blue stick diagrams, are the result of large hyperfine interactions with ^{63}Cu and ^{65}Cu nuclei. These groups have very little angular dependence and their spacing increases from low to high field because of the large hyperfine interaction. Each of the four primary Cu hyperfine lines is further split into many additional superhyperfine lines by an interaction with one boron neighbor (both ^{10}B and ^{11}B lines are resolved). These large Cu hyperfine parameters and their isotropic nature establish that the Cu^0_A and Cu^0_B centers are, to first order, copper atoms. In Fig. 3, the concentration of Cu^0_Acenters is approximately 2.7 times greater than the concentration of Cu^0_B centers, and their combined concentration is approximately 5.5×10^{17} cm^{-3}. This total is about a factor of four lower than the concentration of Cu^{2+}_{active} centers produced by the same irradiation.

Fig. 4 provides an expanded view of the lowest- and highest-field groups of EPR lines associated with the Cu^0_A and Cu^0_B defects. The primary lines can be separated into sets of four based on their relative spacings and intensities, with each set of four due to the interaction with a ^{11}B nucleus. The stick diagrams in Fig. 4 illustrate these sets of four lines, with the red lines representing Cu^0_A and the blue lines representing Cu^0_B. Close inspection of the low-field side of Fig. 4 reveals that the intensity ratio of the two Cu^0_A sets are in good agreement with the ratio of the natural abundance of the two magnetic copper isotopes. Hence, these two sets are labeled ^{63}Cu and ^{65}Cu. Similar analysis of the Cu^0_B center lines shows the same result, and the sets are labeled ^{63}Cu and

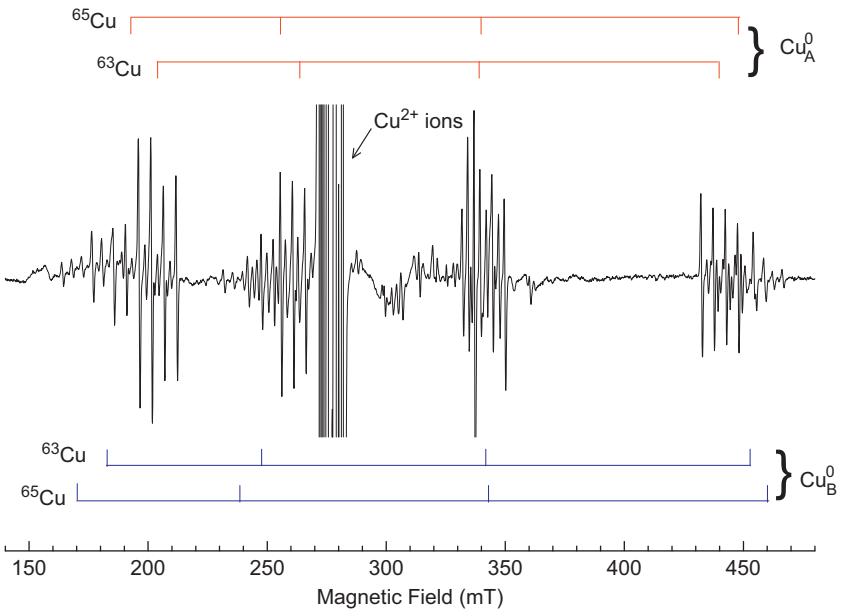

Fig. 3. EPR spectrum showing the Cu_A^0 and Cu_B^0 centers. These data were taken at 45 K with the magnetic field along the [0 0 1] direction. The stick diagrams indicate the midpoints of the sets of ^{63}Cu and ^{65}Cu hyperfine lines for each center (red for the Cu_A^0 center and blue for the Cu_B^0 center). The off-scale signals near 275 mT are from the Cu^{2+}-V_{Li} and Cu_{active}^{2+} centers. (For interpretation of the references to color in this figure legend, the reader is referred to the web version of this article.)

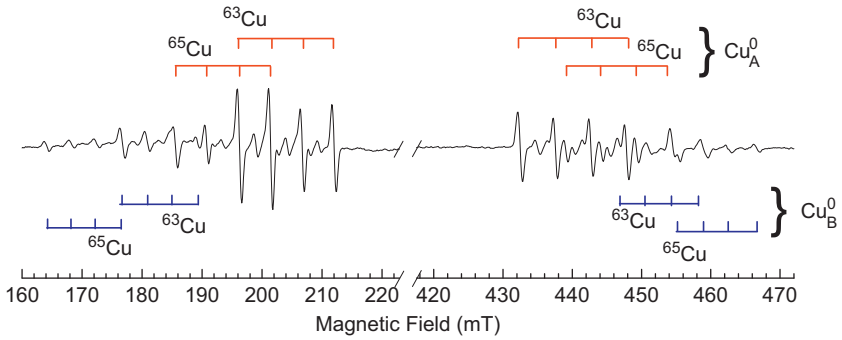

Fig. 4. Expanded view of the lowest and highest field sets of lines in Fig. 3 for the Cu_A^0 and Cu_B^0 centers. This spectrum was taken at 45 K with the magnetic field along the [0 0 1] direction. The stick diagrams indicate the four ^{11}B superhyperfine lines associated with the outer ^{63}Cu and ^{65}Cu lines identified in Fig. 3 (red for the Cu_A^0 center and blue for the Cu_B^0 center). (For interpretation of the references to color in this figure legend, the reader is referred to the web version of this article.)

^{65}Cu. Values for the ^{63}Cu and ^{65}Cu hyperfine parameters are listed in Table 1 for both centers. The isotropic g value of both centers is 2.0023 ± 0.0005. For each center, the ratio of the ^{65}Cu and ^{63}Cu hyperfine parameters is 1.07, in agreement with the ratio of the known magnetic moments of the two Cu isotopes.

In Fig. 4, each copper hyperfine line is split into four lines as a result of a superhyperfine interaction with a nearby ^{11}B nucleus (80.2% abundant, $I=3/2$). The stick diagrams in Fig. 4 are divided into sets of four to reflect this superhyperfine interaction. Additional lines due to a ^{10}B nucleus (19.8% abundant, $I=3$) are easily seen within the group of lines on the low-field side of Fig. 4, and thus verifies that boron is responsible for this superhyperfine interaction. There are small lines near 200, 204, and 210 mT that are part of a set of seven lines from a ^{10}B nucleus. Other lines that are part of this set of seven are barely visible as shoulders near 202 and 209 mT. This pattern of seven lines of small intensity and four lines of larger intensity is consistent with a boron interaction. The magnetic moment of ^{10}B is nearly three times smaller than the magnetic moment of ^{11}B, so the seven ^{10}B superhyperfine lines are expected to appear between the ^{11}B lines. The assignment of boron as the nucleus responsible for the superhyperfine interaction is further supported by the ratio of the splitting between adjacent EPR lines for the two boron isotopes. The average splitting between adjacent ^{10}B lines is 1.842 mT, while the average splitting between adjacent ^{11}B lines is 5.261 mT. The ratio of these average splittings is 2.855, which is in good agreement with the known 2.987 ratio of the ^{10}B and ^{11}B magnetic moments. Only the ^{10}B superhyperfine lines mentioned above are fully visible in Fig. 4; the remaining ^{10}B lines in the Cu_A^0 center as well as all of the ^{10}B lines in the Cu_B^0 center are either overlapped by ^{11}B superhyperfine lines or are too weak to be observed.

In our previous publication describing the identification of silver electron and hole traps in silver-doped $Li_2B_4O_7$ crystals [28], we observed a similar superhyperfine behavior for the interstitial Ag^0 center. The hyperfine lines of the two silver isotopes were each split into four superhyperfine lines, due to an interaction with an $I=3/2$ nucleus. At that time, we could not definitively assign the interaction to a boron nucleus because the ^{10}B lines were not visible. With the information we have obtained in the present study of Cu-doped $Li_2B_4O_7$, we conclude that the additional splitting of silver hyperfine lines in the Ag^0 electron center

Table 1
Spin-Hamiltonian parameters for the Cu^0 electron centers (Cu_A^0 and Cu_B^0) in Cu-doped $Li_2B_4O_7$ crystals.

	g	$A(^{63}Cu)$ $A(^{65}Cu)$
Cu_A^0	2.0023	2178–2333 MHz
Cu_B^0	2.0023	2480–2663 MHz

These values were obtained from the EPR spectrum in Fig. 3. Estimated error limits are ± 0.0005 for the g values and ± 15 MHz for the A values.

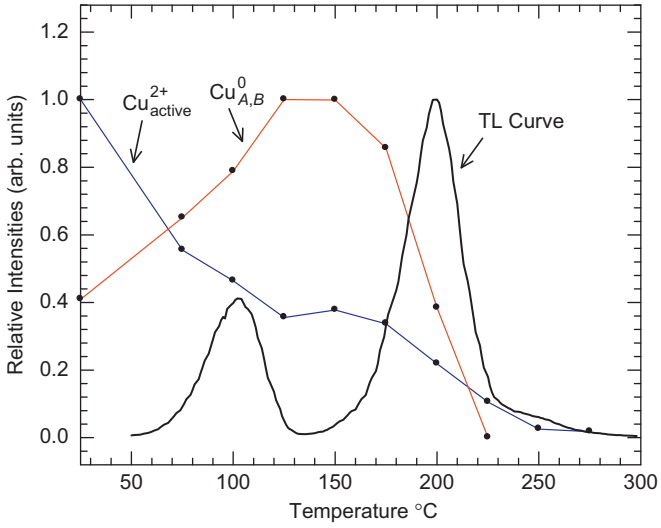

Fig. 5. TL glow curve from a Cu-doped $Li_2B_4O_7$ crystal and the normalized thermal stabilities of the Cu^{2+}_{active} center (blue) and the Cu_A^0 and Cu_B^0 centers (red), as determined by EPR. The EPR data points were obtained by monitoring the signals at 25 K and 45 K, respectively, during a series of pulsed anneals. The effective heating rate during the EPR pulsed anneal experiment was 0.2 °C/s. The TL glow curve (black), also normalized, was obtained by measuring the total light output and using a heating rate of 1 °C/s. (For interpretation of the references to color in this figure legend, the reader is referred to the web version of this article.)

spectrum in silver-doped $Li_2B_4O_7$ is due to an interaction with a neighboring boron nucleus [28].

3.3. *Thermal stability of radiation-induced defects*

The thermal stabilities of the radiation-induced charge states of copper in our $Li_2B_4O_7$ crystals were determined by monitoring their EPR signals during an isochronal pulsed anneal experiment. Fig. 5 shows the changes in concentrations of the Cu^{2+}_{active} centers and the Cu_A^0 and Cu_B^0 centers as a crystal is heated above room temperature after being irradiated with X-rays at room temperature. These annealing curves have been separately normalized to the maximum signals observed. The blue trace is the EPR signal intensity of the Cu^{2+}_{active} center and the red trace is the combined EPR signal intensity of the Cu_A^0 and Cu_B^0 centers. We did not observe a difference in the thermal decay of the Cu_A^0 and Cu_B^0 electron centers, i.e., they have the same thermal stability. The pulsed anneal experiment was carried out using the following procedure. After the crystal was irradiated with x rays for 60 min at room temperature, the EPR signal intensities of the radiation-induced hole and electron centers were recorded at 25 and 45 K, respectively, with the magnetic field aligned along the [1 1 0] direction. The two low-temperature monitoring temperatures are used because the Cu^{2+}_{active} spectrum is best observed at 25 K and the Cu_A^0 and Cu_B^0 spectra are best observed at 45 K. After taking the initial spectra, the crystal was removed from the EPR microwave cavity and placed for two minutes in a furnace that had been preheated to 75 °C. The crystal was then returned to the microwave cavity, and the EPR signal intensities were again recorded at 25 and 45 K. This heating process was repeated at 25 °C intervals from 75 to 275 °C. The "effective" heating rate of the crystal during this pulsed anneal experiment was approximately 0.2 °C/s. As shown in Fig. 5, between room temperature and 125 °C, the concentration of the Cu^{2+}_{active} centers decreases and the combined concentration of the Cu_A^0 and Cu_B^0 centers increases.

A TL glow curve, representing total light output from the Cu-doped $Li_2B_4O_7$ crystal after an X-ray irradiation at room temperature, is also shown in Fig. 5. The heating rate used to obtain this glow curve was 1 °C/s, the slowest rate allowed by our Harshaw reader. Two TL peaks are observed, one near 100 °C and the other near 200 °C. The TL peak near 100 °C occurs in the same temperature range as the initial decay step of the EPR signal from the Cu^{2+}_{active} center. Interestingly, the concentrations of the Cu_A^0 and Cu_B^0 centers increase over this temperature range. The TL peak near 200 °C correlates quite well with the simultaneous thermal decay of the Cu^{2+}_{active} center and the Cu_A^0 and Cu_B^0 centers. There are reports in the literature of the 100 and 200 °C TL peaks in Cu-doped $Li_2B_4O_7$ [14,18,26] and some authors have reported two TL peaks, at slightly different temperatures in crystals doped with manganese [35,36]. Only one above-room-temperature TL peak has been reported for silver-doped $Li_2B_4O_7$ crystals [28].

4. Discussion

The present EPR study shows that our as-grown copper-doped $Li_2B_4O_7$ crystal contains four distinct copper defects. One is a substitutitional Cu^+ ion with no nearby perturbations. A second is a substitutional Cu^{2+} ion adjacent to a lithium vacancy (Cu^{2+}-V_{Li}). The remaining two are interstitial Cu^+ ions in slightly different environments. Of these four, only the Cu^{2+}-V_{Li} center is paramagnetic and thus visible with EPR in the as-grown crystal. Corradi et al. [29] were the first to observe this EPR spectrum in $Li_2B_4O_7$ crystals. More recently, Swinney et al. [27] have shown that large concentrations of lithium and oxygen vacancies are usually present in as-grown undoped $Li_2B_4O_7$ crystals.

When irradiated with X-rays at room temperature, we find that three of these four defects can change charge state. The ionizing radiation produces large concentrations of separated (uncorrelated) electrons and holes in the lattice. Many of these immediately recombine while others become stabilized at trapping sites. During the irradiation, isolated substitutional Cu^+ ions trap holes and convert to Cu^{2+} ions, thus forming the defect we have labeled the Cu^{2+}_{active} center. The Cu^{2+}-V_{Li} centers, on the other hand, do not change charge state during the irradiation. Thus, after the irradiation, two distinct Cu^{2+} EPR spectra are present. The Cu^{2+}_{active} and the Cu^{2+}-V_{Li} spectra occupy the same regions of magnetic field and have significant overlapping of lines for all orientations of the crystal. By comparing spectra taken before and after the irradiation, we are able to identify the lines associated with the Cu^{2+}_{active} center. Although a complete set of angular data was not collected and analyzed, a cursory examination of the spectra at various angles reveals that the spin-Hamiltonian parameters for the two centers differ only slightly. The complete set of parameters for the Cu^{2+}-V_{Li} center have been provided by Corradi et al. [29]. In an earlier study characterizing Ag^{2+} and Ag^0 impurities in silver-doped $Li_2B_4O_7$ [28], an EPR spectrum attributable to a Ag^{2+}-V_{Li} center was not observed in the as-grown crystals. This suggests that our copper-doped $Li_2B_4O_7$ crystals must have a higher concentration of lithium vacancies than the earlier silver-doped crystals.

Also during the irradiation, electrons are trapped at interstitial Cu^+ ions and form two distinct copper atoms, labeled Cu_A^0 and Cu_B^0.

These two centers have slightly different Cu hyperfine constants, presumably because of differing environments. It is possible that the Cu_A^0 and Cu_B^0 centers could be substitutional atoms, i.e., substitutional Cu^+ ions could trap an electron and form substitutional Cu^0 atoms. However, our observation of a significant hyperfine interaction with one boron ion in the Cu_A^0 and Cu_B^0 EPR spectra strongly suggests that these centers occupy interstitial positions. For the Cu_A^0 and Cu_B^0 centers, the unpaired electron occupies a Cu 4s orbital, and this is the reason for the large hyperfine splittings associated with these centers. The measured isotropic ^{63}Cu hyperfine constants of 2178 and 2480 MHz for the Cu_A^0 and Cu_B^0 centers, respectively, are each less than half of the isotropic hyperfine constant of 5995 MHz predicted by Morton and Preston [37] for ^{63}Cu. This means that in each center, approximately 35–40% of the unpaired spin is in a 4s orbital. The remaining spin density is located on the neighboring boron ion (seen in the superhyperfine interaction in Figs. 3 and 4) and on neighboring oxygen ions. The interactions with oxygen nuclei would not produce detectable superhyperfine lines due to the low abundance of the magnetic oxygen isotope (^{17}O: $I=5/2$, 0.038% abundant). A significant overlap of the unpaired spin density onto only one boron ion is not expected if the Cu^0 atom occupies a regular Li^+ site. The distance between a lithium site and its nearest boron neighbors is, on average, about 2.7 Å. For a Cu^0 atom substituting for a Li^+ ion, we expect more of the unpaired spin density to remain in the 4s orbital, and hence, produce a larger isotropic Cu hyperfine parameter than what is observed. The relatively small Cu 4s hyperfine contribution and the significant superhyperfine interaction with one boron nucleus provide strong evidence that the Cu_A^0 and Cu_B^0 centers are interstitial copper defects. Thus, our EPR results agree with the proposal of Corradi et al. [30] that Cu^+ ions occupy interstitial positions in as-grown copper-doped $Li_2B_4O_7$ crystals. These interstitial Cu^+ ions trap electrons and convert to Cu^0 centers during an x-ray irradiation. It is interesting that Cu^+ ions substituting for Li^+ ions do not show amphoteric behavior, i.e., Cu^0 atoms are not produced at substitutional sites during room-temperature irradiations.

Fig. 5 shows the correlation between the thermal stability of the radiation-induced defects, as determined with EPR, and the TL glow peaks in a copper-doped $Li_2B_4O_7$ crystal. The thermal decay of the Cu_{active}^{2+} EPR signal occurs in two distinct steps, one step between room temperature and 125 °C and the other between 150 and 250 °C. The EPR spectra of the Cu_A^0 and Cu_B^0 centers also change in these two temperature regions; their concentrations increase between room temperature and 125 °C and decrease between 150 and 250 °C. Initially, we focus on the second of these two steps, where the simultaneous decrease in EPR signals directly correlates with the TL peak at 200 °C. The EPR results indicate that the Cu_A^0 and Cu_B^0 centers revert to interstitial Cu^+ ions and the Cu_{active}^{2+} centers revert to substitutional Cu^+ ions in this higher temperature range, i.e., electron–hole recombination occurs. We are unable to determine the recombination site because we do not know whether the Cu_{active}^{2+} centers release a hole or the Cu_A^0 and Cu_B^0 centers release an electron. In other words, our data does not distinguish between a hole recombining with an electron at the Cu_A^0 and Cu_B^0 sites or an electron recombining with a hole at the Cu_{active}^{2+} site. The important result is that we have identified the two defects, one electronlike and one holelike, that participate in the recombination process and are responsible for the TL peak near 200 °C.

The recombination step in Fig. 5, occurring between room temperature and 125 °C, coincides with the low-temperature TL peak near 100 °C. A unique feature of this lower-temperature recombination step is the increase in concentration of the Cu_A^0 and Cu_B^0 centers. Their growth eliminates the possibility that electrons are being released from these centers. Also, it appears that holes are not being released from the Cu_{active}^{2+} center in this temperature region, because their release would result in a decrease in the concentration of the Cu_A^0 and Cu_B^0 centers (which is opposite to the observed behavior). The results shown in Fig. 5 suggest that electrons are released from a third unobserved and unidentified defect during this initial recombination step. Some of these electrons released from the third defect recombine with trapped holes at the Cu_{active}^{2+} center and produce the TL peak near 100 °C in Fig. 5. The rest of the electrons released from this third unobserved defect are trapped at interstitial Cu^+ ions and form additional Cu_A^0 and Cu_B^0 centers, thus accounting for the increase in concentration of these two centers. A candidate for this third defect that releases electrons is oxygen vacancies. Using EPR [27], it has previously been shown that oxygen vacancies are incorporated into $Li_2B_4O_7$ crystals during growth and that they trap electrons when the crystal is irradiated with X-rays. Thus far, an EPR signal attributed to oxygen vacancies has not been detected in our Cu-doped samples after an irradiation at room temperature. Because of their lower concentrations compared to copper, it is not likely that trace amounts of other transition-metals ions are this third defect. The release of electrons over this temperature range correlates with the previously observed increase in surface conductivity of Cu-doped $Li_2B_4O_7$ [38].

5. Summary

The complex defect chemistry of copper in $Li_2B_4O_7$ crystals has been clarified in the present study by using the EPR technique. We find that copper can act both as an electron trap and a hole trap in these crystals. Unirradiated as-grown single crystals of copper-doped $Li_2B_4O_7$ contain both nonparamagnetic Cu^+ and paramagnetic Cu^{2+} ions. The Cu^{2+} ions occupy lithium sites, with an adjacent lithium vacancy providing charge compensation (these are referred to as Cu^{2+}-V_{Li} centers). The Cu^+ ions occupy both lithium sites and interstitial positions. During an X-ray irradiation at room temperature, the Cu^+ ions on lithium sites trap holes and convert to Cu^{2+} centers (these are referred to as Cu_{active}^{2+} centers). These Cu_{active}^{2+} centers do not have an adjacent lithium vacancy. At the same time, electrons are trapped at interstitial Cu^+ ions, converting them to paramagnetic Cu^0 atoms (these are referred to as Cu_A^0 and Cu_B^0 centers). The two interstitial centers have slightly different environments and can easily be distinguished in EPR experiments.

Two TL peaks are observed when an irradiated crystal is heated above room temperature. A glow peak near 100 °C occurs when electrons that are thermally released from an unidentified defect recombine with the radiation-induced trapped holes at the Cu_{active}^{2+} center. We tentatively suggest that these unidentified electron traps are oxygen vacancies. Other electrons released from the unidentified electron centers are trapped at the Cu_A^0 and Cu_B^0 centers, as shown by the increase in the Cu_A^0 and Cu_B^0 EPR signals as the crystal goes from room temperature to 125 °C. A second, more intense TL peak near 200 °C is observed in the same temperature range where the EPR signals from the Cu_{active}^{2+} center and the Cu_A^0 and Cu_B^0 centers simultaneously decay. We have not established whether this latter recombination process is initiated by electron release or hole release.

Acknowledgments

One of the authors (ATB) wishes to acknowledge support in the form of a Research Associateship Award from the National Research Council. This work was supported at the Air Force Institute of Technology by the Defense Threat Reduction Agency

(Grant No. HDTRA1-07-1-0008 and BRBAA08-I-2-0128) and at the Institute of Physical Optics by STCU Project 4947.

References

[1] G.D. Patra, M. Tyagi, D.G. Desai, B. Tiwari, S. Sen, S.C. Gadkari, J. Lumin. 132 (2012) 1101.
[2] M. Ignatovych, V. Holovey, T. Vidoczy, P. Baranyai, A. Keleman, Radiat. Phys. Chem. 76 (2007) 1527.
[3] N. Senguttuvan, M. Ishii, M. Shimoyama, M. Kobayashi, N. Tsutsui, M. Nikl, M. Dusek, H.M. Shimizu, T. Oku, T. Adachi, K. Sakai, J. Suzuki, Nucl. Instrum. Methods Phys. Res. A 486 (2002) 264.
[4] M. Ignatovych, V. Holovey, A. Watterich, T. Vidoczy, P. Baranyai, A. Keleman, O. Chuiko, Radiat. Meas. 38 (2004) 567.
[5] M. Ishii, Y. Kuwano, T. Asai, N. Senguttuvan, T. Hayashi, M. Kobayashi, T. Oku, K. Sakai, T. Adachi, H.M. Shimizu, J. Suzuki, J. Cryst. Growth 257 (2003) 169.
[6] G.D. Patra, S.C. Singh, B. Tiwari, S. Sen, D.G. Desai, S.C. Gadkari, J. Lumin. 137 (2013) 28.
[7] V.M. Holovey, K.P. Popovich, D.B. Goyer, V.M. Krasylynets, A.V. Gomonnai, Radiat. Eff. Defects Solids 166 (2011) 522.
[8] K.-S. Park, J.K. Ahn, D.J. Kim, H.K. Kim, Y.H. Hwang, D.S. Kim, M.H. Park, Y. Park, J.-J. Yoon, J.-Y. Leem, J. Cryst. Growth 249 (2003) 483.
[9] D.I. Shahare, B.T. Deshmukh, S.V. Moharil, S.M. Dhopte, P.L. Muthal, V.K. Kondawar, Phys. Status Solidi (a) 141 (1994) 329.
[10] Ya. V. Burak, Ya. O. Dovgyii, I.V. Kityk, Fiz. Tverd. Tela 31 (1989) 275.
[11] O.T. Antonyak, V.T. Adamiv, Ya. V. Burak, I.M. Teslyuk, Funct. Mater. 9 (2002) 452.
[12] N. Can, T. Karali, P.D. Townsend, F. Yildiz, J. Phys D: Appl. Phys. 39 (2006) 2038.
[13] Z. Xiong, Q. Tang, C. Zhang, Sci. China Ser. G: Phys. Mech. Astron. 50 (2007) 311.
[14] V.M. Holovey, V.I. Sidey, V.I. Lyamayev, P.P. Puga, J. Lumin. 126 (2007) 408.
[15] A.S. Pradhan, R.C. Bhatt, K.G. Vohra, Radiochem. Radioanal. Lett. 53 (1982) 103.
[16] J.K. Srivastava, S.J. Supe, J. Phys. D: Appl. Phys. 22 (1989) 1537.
[17] B. Tiwari, N.S. Rawat, D.G. Desai, S.G. Singh, M. Tyagi, P. Ratna, S.C. Gadkari, M.S. Kulkarni, J. Lumin. 130 (2010) 2076.
[18] G.D. Patra, A.K. Singh, S.G. Singh, M. Tyagi, S. Sen, B. Tiwari, S.C. Gadkari, Solid State Physics: in: Proceedings of the 56th DAE Solid State Physics Symposium 2011: AIP Conference Proceedings, vol. 1447, 2012, pp. 1335.
[19] G.I. Malovichko, L.E. Vitruk, N. Yu., Ya. V. Yurchenko, V.G. Burak, A.O. Grachev, D. Matkovskii, Yu. Sugak, Sov. Phys. Solid State 34 (1992) 272.
[20] V. Skvortsova, N. Mironova-Ulmane, U. Ulmanis, A. Matkovskii, Nucl. Instrum. Methods Phys. Res. B 166 (2000) 284.
[21] Ya. V. Burak, B.V. Padlyak, V.M. Shevel, Nucl. Instrum. Methods Phys. Res. B 191 (2002) 633.
[22] Ya. V. Burak, B.V. Padlyak, V.M. Shevel, Radiat. Eff. Defects Solids 157 (2002) 1101.
[23] Sangeeta, K. Chennakesavulu, D.G. Desai, S.C. Sabharwal, M. Alex, M.D. Ghodgaonkar, Nucl. Instrum. Methods Phys. Res. A 571 (2007) 699.
[24] A. Keleman, M. Ignatovych, V. Holovey, T. Vidoczy, P. Baranyai, Radiat. Phys. Chem. 76 (2007) 1531.
[25] Ya. V. Burak, V.T. Adamiv, I.M. Teslyuk, V.M. Shevel, Radiat. Meas. 38 (2004) 681.
[26] M. Takenaga, O. Yamamoto, T. Yamashita, Nucl. Instrum. Methods 175 (1980) 77.
[27] M.W. Swinney, J.W. McClory, J.C. Petrosky, Shan Yang, A.T. Brant, V.T. Adamiv, Ya. V. Burak, P.A. Dowben, L.E. Halliburton, J. Appl. Phys. 107 (2010) 113715.
[28] A.T. Brant, B.E. Kananen, M.K. Murari, J.W. McClory, J.C. Petrosky, V.T. Adamiv, Ya. V. Burak, P.A. Dowben, L.E. Halliburton, J. Appl. Phys. 110 (2011) 093719.
[29] G. Corradi, V. Nagirnyi, A. Kotlov, A. Watterich, M. Kirm, K. Polgar, A. Hofstaetter, M. Meyer, J. Phys.: Condens. Matter 20 (2008) 025216.
[30] G. Corradi, V. Nagirnyi, A. Watterich, A. Kotlov, K. Polgar, J. Phys.: Conf. Ser. 249 (2010) 012008.
[31] J. Krogh-Moe, Acta Crystallogr. 15 (1962) 190.
[32] M.M. Islam, V.V. Maslyuk, T. Bredow, C. Minot, J. Phys. Chem. B 109 (2005) 13597.
[33] N. Sennova, R.S. Bubnova, G. Cordier, B. Albert, S.K. Filatov, L. Isaenko, Z. Anorg. Allg. Chem. 634 (2008) 2601.
[34] V.T. Adamiv, Y.V. Burak, I.M. Teslyuk, J. Alloys Compd. 475 (2009) 869.
[35] E.J. West, A.E. Nash, F.H. Attix, R.D. Kirk, J.H. Schulman, Report of NRL Progress, 1967.
[36] S.W.S. McKeever, Thermoluminescence of Solids, Cambridge University Press, New York, NY, 1985, p. 276.
[37] J.R. Morton, K.F. Preston, J. Magn. Reson. 30 (1978) 577.
[38] J. Xioa, N. Lozova, Ya. B. Losovyj, D. Wooten, I. Ketsman, M.W. Swinney, J.C. Petrosky, J.W. McClory, Ya. V. Burak, V.T. Adamiv, A.T. Brant, P.A. Dowben, Appl. Surf. Sci. 257 (2011) 3399.